Exploiting Residual Edge Information in Deep Fully Convolutional Neural Networks For Retinal Vessel Segmentation

1st Tariq M. Khan
Faculty of Sci Eng & Built Env, School of Info Technology
Deakin University, Geelong Waurn Ponds Campus
Victoria, Australia
tariq045@gmail.com

2nd Syed S. Naqvi
Department of Electrical and Computer Engineering
COMSATS University Islamabad
Islamabad, Pakistan
saud_naqvi@comsats.edu.pk

3rd Muhammad Arsalan
Division of Electronics and Electrical Engineering
Dongguk University
Seoul 100-715, Korea
engineerarsal5@gmail.com

4th Muhamamd Aurangzeb Khan
Computing and Communications
Lancaster University
Lancaster, UK
m.a.khan4@lancaster.ac.uk

5th Haroon A. Khan
Department of Electrical and Computer Engineering
COMSATS University Islamabad
Islamabad, Pakistan
haroon.ahmed@comsats.edu.pk

6th Adnan Haider
Department of Electrical and Computer Engineering
COMSATS University Islamabad
Islamabad, Pakistan
adnanhaider66@gmail.com

***Abstract*—Accurate automatic segmentation of the retinal vessels is crucial for early detection and diagnosis of vision-threatening retinal diseases. A new supervised method using a variant of the fully convolutional neural network is proposed with the advantages of reduced hyper-parameters, reduced computational/memory requirements, and robust performance in capturing tiny vessel information. The fully convolutional architectures previously employed for vessel segmentation have multiple tunable hyperparameters and difficulty in end-to-end training due to their decoder structure. We resolve this problem by sharing information from the encoder for upsampling at the decoder stage, resulting in a significantly smaller number of tunable parameters and low computational overhead at the train and test stages. Moreover, the need for pre- and post-processing steps are eradicated. Consequently, the detection accuracy is significantly improved with scores of 0.9620, 0.9623, and 0.9620 on DRIVE, STARE, and CHASE DB1 datasets respectively.**

***Index Terms*—Retinal vessel segmentation, Deep fully convolutional neural network, Semantic segmentation, Low-level semantic information, Residual edge information**

I. Introduction

Many established eye diseases including retinal vascular occlusions, age-related macular degeneration (AMD), diabetic retinopathy (DR) chronic systematic hypoxemia, and glaucoma can be characterized by appearance changes in retinal blood vessels. Early detection, diagnosis, and tracking of disease progression can prevent vision loss in the case of AMD and DR, and lead to cost-effective treatment options for other conditions [1]–[3]. Therefore, the role of retinal vascular tree segmentation for the implementation of automated retinal screening programs is peerless [4].

Manual delineation requires the images to be manually segmented by trained ophthalmologists or optometrists. It is a tedious, time consuming, and skill demanding task, where there is a fundamental limit on the amount of reliable information that can be extracted from retinal images. In contrast, automatic segmentation algorithms have the potential to be deployed for large public screening with increased accuracy and reduced labor. However, the accuracy of computer algorithms is limited due to the miscellaneous challenges of automatic vessel segmentation.

Automatic vessel segmentation has been widely accepted as a challenging task but is vital for a computer-aided diagnostic system for ophthalmic diseases [5]–[8]. Vessel segmentation is a multifaceted problem that poses several challenges including variation in shape, size, intensity, and direction of vessels [1], [9], [10]. Other difficulties include branching, the crossing of vessels, and the centerline reflex. Moreover, other structures such as an optic disc, macula, pathologies (exudates and lesions), and optic disc boundary add to its complexity. The environmental factors, such as camera acquisition noise, must also be taken into account.

Deep neural networks (DNNs) have achieved state-of-the-art performance in retinal vessel segmentation [11]–[14], which advocates their application to automated retinal image analysis and diagnostics. This performance is achieved at the expense

978-1-7281-6926-2/20/$31.00 ©2020 IEEE

of costly strategies including ensemble networks, pre- and post-processing approaches, and parametric loss functions. These studies ignore important factors such as memory overhead, computational train, test times, and the number of hyper-parameters to tune. Also, effective data augmentation strategies for training DNNs have not been rigorously investigated in the past.

Recently, U-Net based architectures [15]–[17] have shown noteworthy performance in terms of all performance measures on the task of retinal vessel segmentation. The architecture of U-Net is well-suited for medical image segmentation, however, the depth of the architecture and the various stages of processing makes it parameter heavy. In contrast, we present an encoder-decoder based architecture inspired by the network of Badrinarayanan et al. [18]. The proposed network consists of $\sim$7 times lesser parameters as compared to the basic U-Net architecture. Moreover, the proposed network is independent of pre- and post-processing steps. The proposed architecture is found to be better in performance in comparison to the mentioned approaches while having lower memory requirements.

II. Proposed Method

We present an encoder-decoder based fully convolutional architecture for vessel segmentation. The proposed network is inspired by the fully convolutional encoder-decoder architecture of [18]. The details of the proposed convolutional networks are presented in subsequent sections.

A. Vessel Segmentation Using Encoder-Decoder Architecture

The architectural level block diagram of the proposed encoder-decoder fully convolutional neural network is presented in Fig. 1. We call the proposed network VessSeg in this paper. The encoder network consists of 13 convolutional layers similar to the VGG16 network and a corresponding decoder network. The output of the final decoder in the decoder network is fed to a two-class softmax classifier for pixel-wise classification. The output of the softmax classifier is pixel probabilities which categorize pixels either belonging to the vessel or the non-vessel class.

The block-level diagram of one encoder block in the encoder network is presented in Fig. 2. Each individual encoder produces a feature set by convolving the input image with a filter bank. The features are then batch normalized [19] and subsequently subjected to element-wise rectified linear nonlinearity (ReLU) $\max(0; x)$. These resulting maps are then subjected to a stride 2, non-overlapping 2×2 max-pooling windows. While the iterative max-pooling operation allows for increasingly robust classification, the feature maps undergo a loss in spatial resolution due to sub-sampling. This is problematic as boundary details are key to capture blood vessels. An efficient solution to this problem is storing the max-pooling indices in each pooling window per feature map. The output is sub-sampled by a factor of 2, resulting in a larger per-pixel spatial window to obtain the down-sampled feature map.

The VessSeg decoder network starts with the down-sampled feature map produced by the last encoder and successively up-samples it where needed. The up-sampling is achieved by using the max-pooling indices archived by their corresponding encoders. The maps are sparse in nature. The density of the map is increased via convolution using a trainable filter bank. Finally, the dense feature maps are batch normalized. The typical working of a single decoder is summarized in Fig. 3. Each decoder feeds the next decoder and so on repeating the same process. The produced feature maps are consistent in channel size and number to their equivalent encoder inputs. However, the last decoder corresponding to the first encoder is an exception. While the input to the first encoder is a 3 channel RGB image, the output produced by the last decoder is a multi-channel feature map. Each individual pixel of this high dimensional feature representation is classified as either "vessel" or "non-vessel". Each pixel is classified independently using a trainable soft-max classifier. The output is an image of probabilities with two channels corresponding to the two classes. The prediction of the resulting segmentation is based on the class with the highest probability.

B. Training of Networks

Owing to the limited number of annotations in all datasets for the segmentation task, we perform task-dependent data augmentation. As the vessels naturally occur at varying orientations in the vascular structure, we rotate the image at numerous orientations to enhance the generalization of the proposed approach. Besides orientation, the contrast and the illumination variations in fundus images affect the generalization of the network. Therefore, we perform contrast and illumination adjustment to improve the generalization ability of the proposed network in addition to exposing it to images with systematically introduced noise. Stochastic gradient descent with a fixed learning rate of 0.001 was used as the optimizer for training. A batch size of 5 images was used to train the VessSeg network.

The objective function used to train the networks was a cross-entropy loss. The cross-entropy loss defined as $-(ylog(p) + (1 - y)log(1 - p))$ is a probability function for probability p that increases (tends to 1) as the predicted class diverges from the actual class. The losses are summed up over all the pixels. Inherently for the problem of vessel segmentation, the "non-vessel" pixels in every retinal image massively outweigh the "vessel" pixels. This large variation in pixel count between classes can be problematic when the cross-entropy loss is used for training. This problem can be mitigated using class balancing. In class balancing, weights are assigned to every class in the loss function, in such a way that the high-frequency classes have low weights and vice-versa. There are a number of ways that these weights can be assigned. For the purpose of training VessSeg architectures, the weights were derived using median frequency balancing [20]. The weights for each class were computed by dividing the median of class frequencies over the entire training set by the class frequency. As a result of frequency balancing,

978-1-7281-6926-2/20/$31.00 ©2020 IEEE

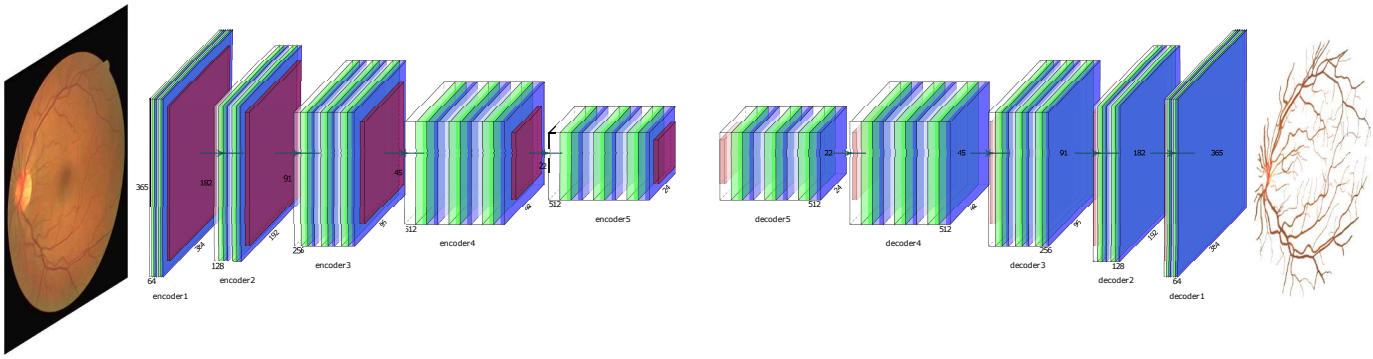

Fig. 1. Block diagram of VessSeg-1.

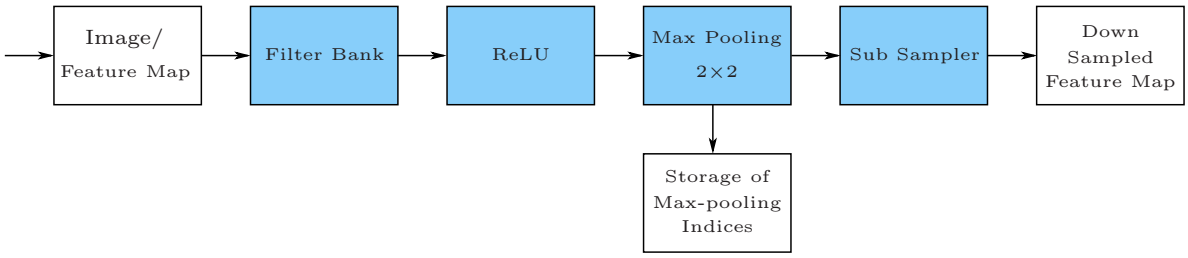

Fig. 2. One encoder in the encoder network.

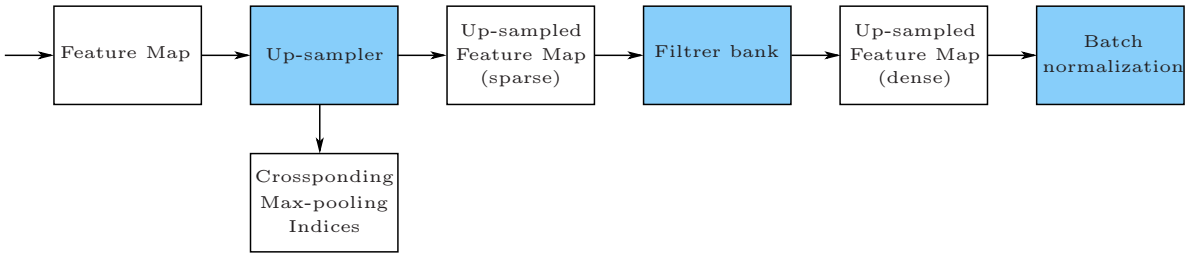

Fig. 3. One decoder in the decoder network.

the "non-vessel" class achieved a weight of 0.577 while the "vessel" class 3.72.

C. Hyperparameter Tuning

Table I presents the hyperparameter settings for the VessSeg network. The weights and biases were initialized using the VGG16 weights. The mini-batch size and the learning rate decay λ were determined empirically in terms of minimal resulting cross-validation loss.

TABLE I
HYPERPARAMETER SETTINGS FOR VESSSEG-1 AND VESSSEG-2 ARCHITECTURES.

Stage	Hyperparameter	VessSeg-1	VessSeg-2
Initialization	Bias	VGG16	VGG16
	Weights	VGG16	VGG16
Training	Epochs	60	40
	Mini-batch size	5	6
	Learning rate decay λ	0.0005	0.0005

III. Experimental Results

A. Materials

The proposed method was evaluated on standard publicly available retinal vessel segmentation datasets including CHASE_DB1: Individual retinal images of both eyes of 14 pediatric subjects [21], Digital Retinal Images for Vessel Extraction (DRIVE): Retinal images of diabetic patients over a wide age range, collected in the Netherlands [22] and Structured Analysis of the Retina (STARE): A set of 20 images from a total of 400 retinal images collected in the USA [23].

In DRIVE, the vessel trees are manually segmented in each available image. Furthermore, each image is accompanied

978-1-7281-6926-2/20/$31.00 ©2020 IEEE

by a binary mask demarcating the field of view (FOV) area. Unlike DRIVE, binary FOV masks are not available for STARE and CHASE_DB1. Consequently, their respective masks must be generated using existing techniques [24]. It is important to note that the sample input patches may be from any part of the image and not confined within the mask. However, the network is expected to learn to distinguish between the edges of the mask and the blood vessels in the retina.

The DRIVE and CHASE_DB1 databases have separate sets for training and testing. However, this is not the case with the STARE data set. A selection of random images from the dataset can be used for training, which is not an unprecedented approach. This technique has been shown to be viable when training and testing data are not separately provided. However, due to data overlap, the results are unrealistically optimistic [25], [26]. A "leave-one-out" approach has been shown to deliver relatively reliable outcomes [22], [24]. In this technique, for a dataset of size 'n', the system is trained using n-1 samples and tested on the one remaining sample, so that there is no overlap. This process is repeated 'n' number of times, "leaving out" each sample in the dataset at least once. This study used the "leave-one-out" approach for training the system using the STARE dataset.

B. Evaluation Criterion

Vessel segmentation algorithms can be considered as binary classifiers that are designed to distinguish between vessels and non-vessels. Their performance is evaluated by comparing their results with the "ground truth". The ground truth is a set of images that are annotated manually by human observers. The following four parameters can be extracted by comparing the algorithm output with the ground truth:

1) True Positive (TP): when vessels are rightfully predicted to be vessels
2) False Negative (FN): when vessels are predicted to be non-vessels
3) True Negative (TN): When non-vessels are correctly identified as non-vessels &
4) False Positive (FP): When non-vessels are denoted to be vessels

These parameters can be used to evaluate the quality of the segmentation algorithm for the pixels inside the FOV as follows above [28]:

$$Se = \frac{TP}{TP+FN},$$
$$Sp = \frac{TN}{TN+FP},$$
$$Acc = \frac{TP+TN}{TP+FN+TN+FP},$$

Here, Se is the sensitivity, indicating how well the classifier can identify vessel pixels. Sp is the specificity, which is the ability of the classifier to identify non-vessel pixels. Acc is the accuracy of the segmentation algorithm, reflecting the ratio between the collection of all correctly classified pixels (vessels or non-vessels) to all the pixels in the field of view described by the mask.

FPR is the fraction of pixels wrongly classified as vessels and is equal to $1 - Sp$. A receiver operating characteristic (ROC) curve is plotted with Se versus FPR while changing the threshold on the probability map due to the quantitative measure's reliance on the threshold. The performance of the methods is also evaluated in the area under the ROC curve (AUC). In the case of an ideal classifier, the AUC should always be equal to 1.

C. Comparison with state-of-the-art

A comprehensive comparison of the proposed VessSeg method is presented with 19 unsupervised and supervised state-of-the-art methods on the DRIVE database, 8 state-of-the-art methods on the CHASE_DB1 database, and 14 methods on the STARE database. Qualitative and quantitative comparison results obtained by the benchmark methods in comparison to the proposed method are shown in Figs. 4, 5, 6 and Tables II, III, IV. The visual results on the DRIVE database in Fig. 4 show that the proposed method captures tiny vessels that are missed by the approach of [27]. Also, the pathological noise and the part of the optic disc erroneously included by the output of Orlando et al. [27] in test images 8 and 14 are successfully suppressed by the proposed method. The visual results on the CHASE_DB1 dataset in Fig. 5 clearly demonstrate that the output of the proposed method is in high agreement with the ground truth, where the approach of Orlando et al. struggles to suppress pathological noise and the optic disc boundary. Fig. 6 exhibits zoomed regions of the images containing pathologies and the corresponding outputs of the methods. The noise suppression ability and the sensitivity to tiny vessels of the proposed approach are further confirmed by the visual outputs in Fig. 6.

The quantitative comparison of the proposed approach in terms of described performance measures with benchmark methods is presented in Tables II, III, IV for the selected datasets. The highest three values for each performance measure in the tables are color-coded, where red is used to represent the highest score, green color represents the second-highest score while the third-highest score is depicted in blue. As per Table II for the DRIVE dataset, the proposed method obtained better results as compares to the unsupervised methods with performance improvements of 2.63% and 0.18% in terms of Se and Acc in comparison to the best-performing unsupervised method. The proposed method also exhibits better performance as compared to methods that employ pre-processing [12] and the parameter heavy U-Net variants [15], [16]. The proposed method outperformed all the supervised methods in terms of Se, Acc, and AUC on the DRIVE dataset. Performance improvements of 8.7% and 1.8% in terms of Se and Acc can be observed in comparison to the best performing unsupervised method on the CHASE_DB1 dataset in Table. III. The proposed VessSeg model obtained better or at par performance as compared to the supervised methods on the CHASE images. It is noteworthy that the proposed

978-1-7281-6926-2/20/$31.00 ©2020 IEEE

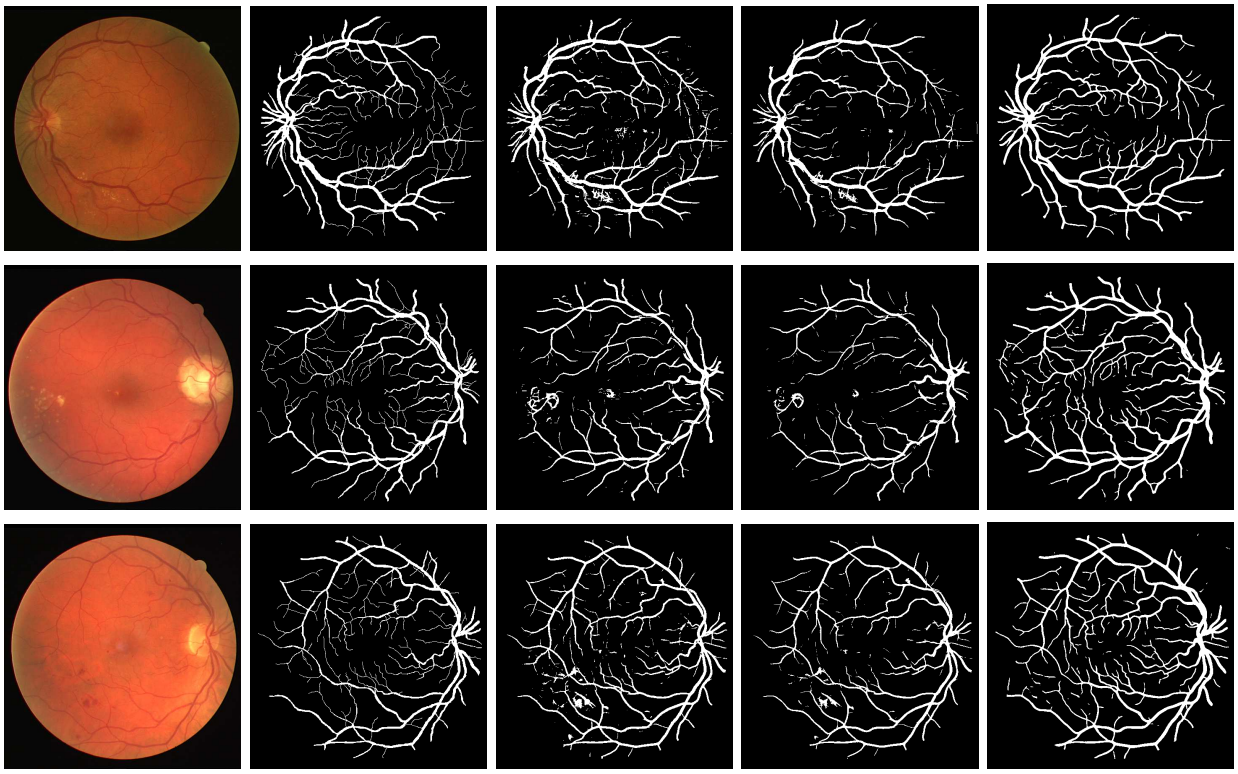

Fig. 4. Analysis of Segmented Output of three sample images (test image 3, 8, 14) of DRIVE dataset. Second column shows the ground truth images. Column 3 and 4 shows the output of [27] UP and [27] FC , respectively. The visual output of the proposed method is shown in the last column.

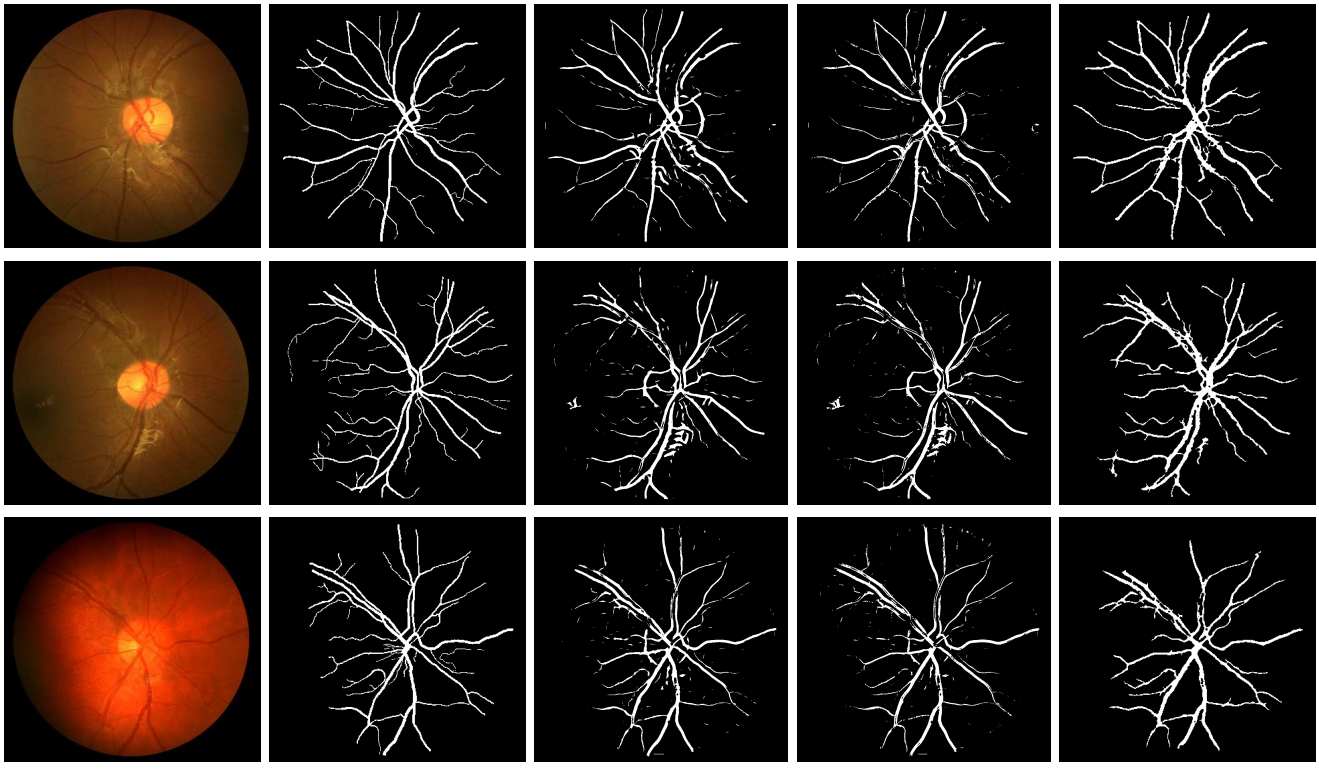

Fig. 5. Analysis of segmented output of three sample images (image 25, 26, 28) of CHASE_DB1 dataset. Second column shows the ground truth images. Column 3 and 4 shows the output of [27] UP and [27] FC , respectively. Column 5 shows the output of the proposed VessSeg architecture.

978-1-7281-6926-2/20/$31.00 ©2020 IEEE

TABLE II
COMPARISON WITH STATE-OF-THE-ART METHODS ON THE DRIVE DATASET.

Type	Methods	Year	Se	Sp	Acc	AUC
Unsupervised methods	Zhang [29]	2016	0.7743	0.9725	0.9476	
	Aguiree [30]	2018	0.7854	0.9662	0.950	
	Khan [31]	2018	0.730	0.979	0.958	
	Khawaja (CLAHE) [32]	2019	**0.8027**	0.9733	0.9561	
	Khawaja (GLM) [32]	2019	0.7907	0.9790	**0.9603**	
	Khawaja [33]	2019	**0.8043**	0.9730	0.9553	
	Zhou [34]	2020	0.7262	0.9803	0.9475	
Supervised methods	Marin et al. [35]	2011	0.7067	0.9801	0.9452	0.9588
	Fraz et al. [36]	2012	0.7406	0.9807	0.9480	0.9747
	Cheng et al. [26]	2014	0.7252	0.9798	0.9474	0.9648
	Li et al. [12]	2016	0.7569	0.9816	0.9527	0.9738
	Orlando et al. [27] FC	2017	0.7893	0.9792	N.A	0.9507
	Orlando et al. [27] UP	2017	0.7076	**0.9870**	N.A	0.9474
	Dasgupta and Singh [37]	2017	0.9691	0.9801	0.9533	0.9744
	Yan et al. [38]	2018	0.7653	**0.9818**	0.9542	**0.9752**
	Olaf et al. [15] U-Net	2018	0.7537	**0.9820**	0.9531	**0.9755**
	Azad et al. [16] BCDU-Net	2019	0.8007	0.9786	0.9560	**0.9798**
	Soomro et al. [39] Strided U-Net	2019	0.8020	0.9740	**0.9590**	0.9480
	Proposed (VessSeg)	2020	**0.8255**	0.9760	**0.9620**	0.9730

TABLE III
COMPARISON WITH STATE-OF-THE-ART METHODS ON THE CHASE_DB1 DATASET

Type	Methods	Year	Se	Sp	Acc	AUC
Unsupervised methods	Roychowdhury et al. [40]	2015	0.7615	0.9575	0.9467	0.9623
	Azzopardi et al. [41]	2015	0.7585	0.9587	0.9387	0.9487
	Zhang et al. [28]	2016	0.7626	0.9661	0.9452	0.9606
Supervised methods	Fraz et al. [36]	2012	0.7224	0.9711	0.9569	0.9712
	Li et al. [12]	2015	0.7507	**0.9793**	**0.9581**	0.9716
	Orlando et al. [27] FC	2017	0.7277	0.9712	N.A	N.A
	Yan et al. [38]	2018	**0.7633**	**0.9809**	**0.9610**	**0.9781**
	Olaf et al. [15] U-Net	2018	**0.8288**	0.9701	0.9578	**0.9772**
	Proposed (VessSeg)	2020	**0.8291**	**0.9730**	**0.9620**	**0.9765**

method obtained comparable performance as compared with the U-Net variants despite having an order of magnitude lesser parameters. Similar results were obtained on the STARE database as evident from Table IV.

The average time required to segment one image on a PC (Intel Core i7, 2.21 GHz with 16GB RAM) is approximately 3 seconds for VessSeg. The method is implemented using MATLAB2017a. For GPU (NVIDIA GTX1070, 8GB), the VessSeg-1's average time is 400 millisecond while VessSeg-2 takes only 300 milliseconds on average to process one image. The average time required to train the network for one dataset is approximately 8 hours for VessSeg. In terms

TABLE IV
COMPARISON WITH STATE-OF-THE-ART METHODS ON THE STARE DATASET

Type	Methods	Year	Se	Sp	Acc	AUC
Unsupervised methods	Zhang [29]	2016	0.7791	0.9758	0.9554	
	Aguiree [30]	2018	0.7116	0.9454	0.9231	
	Khan [31]	2018	0.790	0.965	0.951	
	Khawaja (CLAHE) [32]	2019	0.7980	0.9732	0.9561	
	Khawaja (GLM) [32]	2019	0.7860	0.9725	0.9583	
	Khawaja [33]	2019	**0.8011**	0.9694	0.9545	
Supervised methods	Marin et al. [35]	2011	0.6944	0.9819	0.9526	0.9769
	Fraz et al. [36]	2012	0.7548	0.9763	0.9534	0.9768
	Li at al. [12]	2016	0.7726	**0.9844**	**0.9628**	**0.9879**
	Orlando et al. [27] FC	2017	0.7680	0.9738	N.A	N.A
	Orlando et al. [27] UP	2017	0.7692	0.9675	N.A	N.A
	Yan et al. [38]	2018	0.7581	**0.9846**	0.9612	**0.9801**
	Olaf et al. [15] U-Net	2018	**0.8270**	**0.9842**	**0.9690**	**0.9898**
	Azad et al. [16] BCDU-Net	2019	0.7699	0.9833	0.9574	0.9787
	Soomro et al. [39] Strided U-Net	2019	0.8010	0.9690	0.9610	0.9450
	Proposed (VessSeg)	2020	**0.8318**	0.9758	**0.9623**	0.9758

TABLE V
AVERAGE TIME FOR PROCESSING ONE IMAGE

Type	Methods	Year	Processing time
Unsupervised methods	Jiang and Mojon [42]	2003	10 s
	Mendonca and Campilho [43]	2006	2.5 min
	Al-Diri et al. [44]	2009	11 min
	Azzopardi et al. [41]	2015	10 s
Supervised methods	Staal et al. [22]	2004	15 min
	Soares et al. [24]	2006	3 min
	Martin et al. [35]	2011	1.5 min
	Fraz et al. [36]	2012	2 min
	Li et al. [12]	2015	1.2 min
	VessSeg (PC)	2020	3 s
	VessSeg (GPU)	2020	400 ms

of processing time (Table V), the proposed method has a lower computational complexity in comparison to published algorithms, owing to its lower memory requirements and a lesser number of parameters.

IV. CONCLUSIONS

This work introduced a new model for the task of retinal vessel segmentation. It was established through the analysis of the activation layers of the proposed network that preserving low-level edge information from early convolution layers can aid the networks in robust tiny vessel information detection and help in an overall boost of the performance. The performance of the proposed method on images with pathologies was observed to be more convincing than the performance of the state-of-the-art. The performance of the proposed method as found to be considerably better as compared with the current state-of-the-art in terms of specificity, accuracy, and especially the area under the ROC curve. Considering the robustness of the proposed method to tiny vessel information, pathological images, and real-time computation overhead motivates their application in retinal image diagnosis systems.

We believe that further architectural considerations, such as residual connections between inner convolutional and de-convolutional layers, can provide further insights and lead to further performance improvements in the future. With reference to wide-field imaging, architectural modifications to handle higher resolution images and more detailed vessel structures and pathologies are two subjects of our future research. Deployment of the current method in real-time screening and diagnosis is also to be achieved in the future.

REFERENCES

[1] T. A. Soomro, T. Mahmood Khan, M. A. U. Khan, J. Gao, M. Paul, and L. Zheng, "Impact of ica-based image enhancement technique on retinal blood vessels segmentation," *IEEE Access*, vol. 6, pp. 3524–3538, 2018.

[2] Mohammad AU Khan, Tariq M Khan, Syed S Naqvi, and M Aurangzeb Khan, "Ggm classifier with multi-scale line detectors for retinal vessel segmentation," *Signal, Image and Video Processing*, vol. 13, no. 8, pp. 1667–1675, 2019.

[3] Mohammad AU Khan, Tariq M Khan, Toufique Ahmed Soomro, Nighat Mir, and Junbin Gao, "Boosting sensitivity of a retinal vessel segmentation algorithm," *Pattern Analysis and Applications*, vol. 22, no. 2, pp. 583–599, 2019.

978-1-7281-6926-2/20/$31.00 ©2020 IEEE

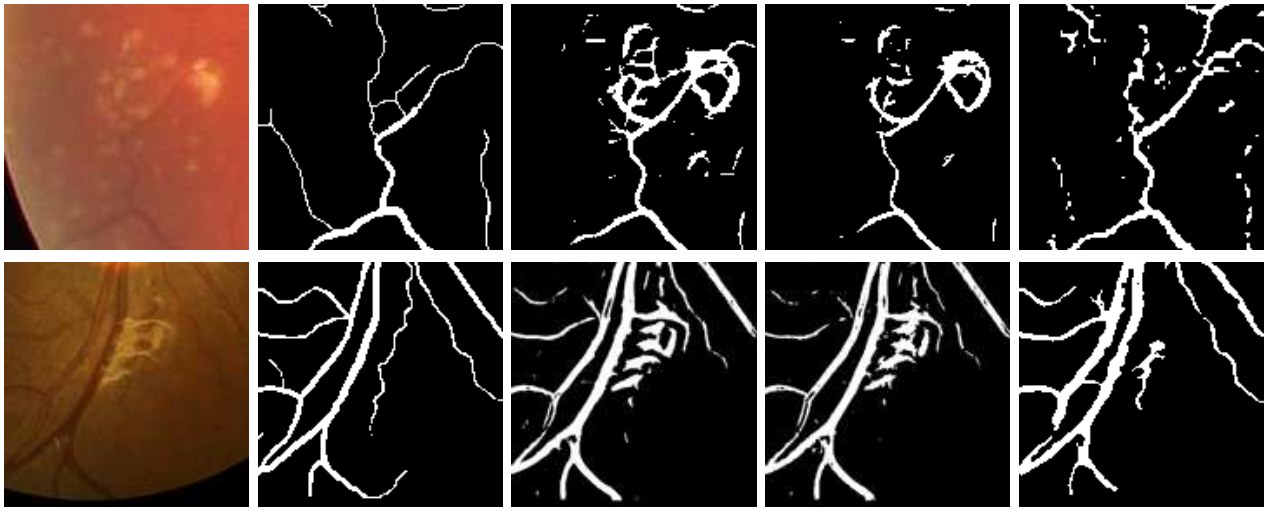

Fig. 6. Performance analysis of proposed method with [27] UP and [27] FC. Column 1 shows sample input images of pathologies and tiny vessels. Columns 2 shows ground images. Column 3 and column shows the output of Orlando FC and Orlando Up [27] respectively. Column 5 shows the output of the proposed VessSeg method.

[4] Mehwish Mehmood, Tariq M Khan, Mohammad AU Khan, Syed S Naqvi, and Wadee Alhalabi, "Vessel intensity profile uniformity improvement for retinal vessel segmentation," *Procedia Computer Science*, vol. 163, pp. 370–380, 2019.

[5] C. Kirbas and F. Quek, "A review of vessel extraction techniques and algorithms," *ACM Comput. Surv.*, vol. 36, no. 2, pp. 81–121, 2004.

[6] Mohammad A.U. Khan Tariq M. Khan Manoranjan Paul Nighat Mir Toufique Soomro, Junbin Gao, "Role of image contrast enhancement technique for ophthalmologist as a diagnostic tool for the diabetic retinopathy," in *IEEE International Conference on Digital Image Computing: Techniques and Applications (DICTA), At Gold Coast, Autralia*, 2016, pp. 1–8.

[7] Toufique Ahmed Soomro, Junbin Gao, Tariq Khan, Ahmad Fadzil M Hani, Mohammad AU Khan, and Manoranjan Paul, "Computerised approaches for the detection of diabetic retinopathy using retinal fundus images: a survey," *Pattern Analysis and Applications*, vol. 20, no. 4, pp. 927–961, 2017.

[8] Toufique Ahmed Soomro, Mohammad AU Khan, Junbin Gao, Tariq M Khan, and Manoranjan Paul, "Contrast normalization steps for increased sensitivity of a retinal image segmentation method," *Signal, Image and Video Processing*, vol. 11, no. 8, pp. 1509–1517, 2017.

[9] Mohammad AU Khan, Tariq M Khan, Kahtan I Aziz, Sayed S Ahmad, Nighat Mir, and Emhemed Elbakush, "The use of fourier phase symmetry for thin vessel detection in retinal fundus images," in *2019 IEEE International Symposium on Signal Processing and Information Technology (ISSPIT)*. IEEE, 2019, pp. 1–6.

[10] Mohammad AU Khan, Tariq M Khan, DG Bailey, and Toufique A Soomro, "A generalized multi-scale line-detection method to boost retinal vessel segmentation sensitivity," *Pattern Analysis and Applications*, vol. 22, no. 3, pp. 1177–1196, 2019.

[11] P. Liskowski and K. Krawiec, "Segmenting retinal blood vessels with deep neural networks," *IEEE Transactions on Medical Imaging*, vol. 35, no. 11, pp. 2369–2380, 2016.

[12] Q. Li, B. Feng, L. Xie, P. Liang, H. Zhang, and T. Wang, "A cross-modality learning approach for vessel segmentation in retinal images," *IEEE Transactions on Medical Imaging*, vol. 35, no. 1, pp. 109–118, 2016.

[13] S. Wang, Y. Yin, G. Cao, B. Wei, Y. Zheng, and G. Yang, "Hierarchical retinal blood vessel segmentation based on feature and ensemble learning," *Neurocomputing*, vol. 149, pp. 708 – 717, 2015.

[14] Muhammad Imran Razzak, Saeeda Naz, and Ahmad Zaib, "Deep learning for medical image processing: Overview, challenges and the future," in *Classification in BioApps*, pp. 323–350. Springer, 2018.

[15] Olaf Ronneberger, Philipp Fischer, and Thomas Brox, "U-net: Convolutional networks for biomedical image segmentation," in *Medical Image Computing and Computer-Assisted Intervention – MICCAI 2015*, Nassir Navab, Joachim Hornegger, William M. Wells, and Alejandro F. Frangi, Eds., Cham, 2015, pp. 234–241, Springer International Publishing.

[16] Reza Azad, Maryam Asadi-Aghbolaghi, Mahmood Fathy, and Sergio Escalera, "Bi-directional convlstm u-net with densley connected convolutions," *CoRR*, vol. abs/1909.00166, 2019.

[17] Md Zahangir Alom, Chris Yakopcic, Mahmudul Hasan, Tarek M. Taha, and Vijayan K. Asari, "Recurrent residual U-Net for medical image segmentation," *Journal of Medical Imaging*, vol. 6, no. 1, pp. 1 – 16, 2019.

[18] V. Badrinarayanan, A. Kendall, and R. Cipolla, "Segnet: A deep convolutional encoder-decoder architecture for image segmentation," *IEEE Transactions on Pattern Analysis and Machine Intelligence*, vol. 39, no. 12, pp. 2481–2495, 2017.

[19] Sergey Ioffe and Christian Szegedy, "Batch normalization: Accelerating deep network training by reducing internal covariate shift," in *Proceedings of the 32Nd International Conference on International Conference on Machine Learning - Volume 37*, 2015, ICML'15, pp. 448–456.

[20] David Eigen and Rob Fergus, "Predicting depth, surface normals and semantic labels with a common multi-scale convolutional architecture," in *Proceedings of the 2015 IEEE International Conference on Computer Vision (ICCV)*, 2015, pp. 2650–2658.

[21] M. M. Fraz, P. Remagnino, A. Hoppe, B. Uyyanonvara, A. R. Rudnicka, C. G. Owen, and S. A. Barman, "Blood vessel segmentation methodologies in retinal images - A survey," *Computer Methods and Programs in Biomedicine*, vol. 108, no. 1, pp. 407–433, 2012.

[22] J. Staal, M. D. Abramoff, M. Niemeijer, M. A. Viergever, and B. van Ginneken, "Ridge-based vessel segmentation in color images of the retina," *IEEE Transactions on Medical Imaging*, vol. 23, no. 4, pp. 501–509, 2004.

[23] A. D. Hoover, V. Kouznetsova, and M. Goldbaum, "Locating blood vessels in retinal images by piecewise threshold probing of a matched filter response," *IEEE Transactions on Medical Imaging*, vol. 19, no. 3, pp. 203–210, 2000.

[24] J. V. B. Soares, J. J. G. Leandro, R. M. Cesar, H. F. Jelinek, and M. J. Cree, "Retinal vessel segmentation using the 2-d gabor wavelet and supervised classification," *IEEE Transactions on Medical Imaging*, vol. 25, no. 9, pp. 1214–1222, 2006.

[25] E. Ricci and R. Perfetti, "Retinal blood vessel segmentation using line operators and support vector classification," *IEEE Transactions on Medical Imaging*, vol. 26, no. 10, pp. 1357–1365, 2007.

[26] E. Cheng, L. Du, Y. Wu, Y. J. Zhu, V. Megalooikonomou, and H. Ling, "Discriminative vessel segmentation in retinal images by fusing context-aware hybrid features," *Machine Vision and Applications*, vol. 25, no. 7, pp. 1779–1792, Oct. 2014.

[27] J. I. Orlando, E. Prokofyeva, and M. B. Blaschko, "A discriminatively trained fully connected conditional random field model for blood vessel

978-1-7281-6926-2/20/$31.00 ©2020 IEEE

segmentation in fundus images," *IEEE Transactions on Biomedical Engineering*, vol. 64, no. 1, pp. 16–27, 2016.
[28] J. Zhang, B. Dashtbozorg, E. Bekkers, J. P. W. Pluim, R. Duits, and B. M. Romeny, "Robust retinal vessel segmentation via locally adaptive derivative frames in orientation scores," *IEEE Transactions on Medical Imaging*, vol. 35, no. 12, pp. 2631–2644, 2016.
[29] Jiong Zhang, Behdad Dashtbozorg, Erik Bekkers, Josien PW Pluim, Remco Duits, and Bart M ter Haar Romeny, "Robust retinal vessel segmentation via locally adaptive derivative frames in orientation scores," *IEEE transactions on medical imaging*, vol. 35, no. 12, pp. 2631–2644, 2016.
[30] Hugo Aguirre-Ramos, Juan Gabriel Avina-Cervantes, Ivan Cruz-Aceves, José Ruiz-Pinales, and Sergio Ledesma, "Blood vessel segmentation in retinal fundus images using gabor filters, fractional derivatives, and expectation maximization," *Applied Mathematics and Computation*, vol. 339, pp. 568–587, 2018.
[31] Khan Bahadar Khan, Amir A Khaliq, Abdul Jalil, and Muhammad Shahid, "A robust technique based on glm and frangi filter for retinal vessel extraction and denoising," *PloS one*, vol. 13, no. 2, pp. e0192203, 2018.
[32] A. Khawaja, T. M. Khan, K. Naveed, S. S. Naqvi, N. U. Rehman, and S. Junaid Nawaz, "An improved retinal vessel segmentation framework using frangi filter coupled with the probabilistic patch based denoiser," *IEEE Access*, vol. 7, pp. 164344–164361, 2019.
[33] Ahsan Khawaja, Tariq M. Khan, Mohammad A. U. Khan, and Syed Junaid Nawaz, "A multi-scale directional line detector for retinal vessel segmentation," *Sensors*, vol. 19, no. 22, 2019.
[34] Chao Zhou, Xiaogang Zhang, and Hua Chen, "A new robust method for blood vessel segmentation in retinal fundus images based on weighted line detector and hidden markov model," *Computer Methods and Programs in Biomedicine*, vol. 187, pp. 105231, 2020.
[35] D. Marin, A. Aquino, M. E. Gegundez-Arias, and J. M. Bravo, "A new supervised method for blood vessel segmentation in retinal images by using gray-level and moment invariants-based features," *IEEE Transactions on Medical Imaging*, vol. 30, no. 1, pp. 146–158, 2011.
[36] Fraz M. M., Remagnino P., Hoppe A., Uyyanonvara B., Rudnicka A. R., Owen C. G., and Barman S. A., "An ensemble classification-based approach applied to retinal blood vessel segmentation," *IEEE Transactions on Biomedical Engineering*, vol. 59, no. 9, pp. 2538–2548, 2012.
[37] A. Dasgupta and S. Singh, "A fully convolutional neural network based structured prediction approach towards the retinal vessel segmentation," in *IEEE 14th International Symposium on Biomedical Imaging (ISBI 2017)*, 2017, pp. 248–251.
[38] Z. Yan, X. Yang, and K. T. Cheng, "Joint segment-level and pixel-wise losses for deep learning based retinal vessel segmentation," *IEEE Transactions on Biomedical Engineering*, pp. 1–1, 2018.
[39] T. A. Soomro, A. J. Afifi, A. Ali Shah, S. Soomro, G. A. Baloch, L. Zheng, M. Yin, and J. Gao, "Impact of image enhancement technique on cnn model for retinal blood vessels segmentation," *IEEE Access*, vol. 7, pp. 158183–158197, 2019.
[40] S. Roychowdhury, D. D. Koozekanani, and K. K. Parhi, "Blood vessel segmentation of fundus images by major vessel extraction and subimage classification," *IEEE Journal of Biomedical and Health Informatics*, vol. 19, no. 3, pp. 1118–1128, 2015.
[41] G. Azzopardi, N. Strisciuglio, M. Vento, and N. Petkov, "Trainable COSFIRE filters for vessel delineation with application to retinal images," *Medical Image Analysis*, vol. 19, no. 1, pp. 46–57, 2015.
[42] X. Jiang and D. Mojon, "Adaptive local thresholding by verification-based multithreshold probing with application to vessel detection in retinal images," *IEEE Transactions on Pattern Analysis and Machine Intelligence*, vol. 25, no. 1, pp. 131–137, 2003.
[43] A. M. Mendonca and A. Campilho, "Segmentation of retinal blood vessels by combining the detection of centerlines and morphological reconstruction," *IEEE Transactions on Medical Imaging*, vol. 25, no. 9, pp. 1200–1213, 2006.
[44] B. Al-Diri, A. Hunter, and D. Steel, "An active contour model for segmenting and measuring retinal vessels," *IEEE Transactions on Medical Imaging*, vol. 28, no. 9, pp. 1488–1497, 2009.

978-1-7281-6926-2/20/$31.00 ©2020 IEEE